EasyChair Preprint

№ 9568

Effect of Flux Composition on Refining and Reoxidation Behavior of Si-Killed Stainless Steel During Ladle and Tundish Metallurgy

Shengchao Duan, Taesung Kim, Jinhyung Cho and Joohyun Park

January 12, 2023

4th International Conference on Science and Technology of Ironmaking and Steelmaking
13-16 Dec. 2022
IIT Bombay, Mumbai, India

Effect of flux composition on refining and reoxidation behavior of Si-killed stainless steel during ladle and tundish metallurgy

Shengchao Duan, Taesung Kim, Jin Hyung Cho, Joo Hyun Park*
Department of Materials Science and Chemical Engineering, Hanyang University, Ansan 15588, Korea
2. Research & Development Center, Hyundai Steel, Dangjin 31719, Korea

* Corresponding author: basicity@hanyang.ac.kr (J. H. Park)

Abstract

The effect of slag composition on the refining and reoxidation behavior of Si-killed 316L stainless steel during ladle and tundish processes were investigated in an induction furnace equipped with a MgO crucible under high purity Ar atmosphere at 1873 K and 1773 K, respectively. For the ladle refining process, the total oxygen (T.O.) content decreased with increasing the Vee ratio (CaO/SiO_2=C/S, 1.0, 1.3, 1.7, and 2.3) of the CaO-SiO_2-Al_2O_3-MgO-CaF_2 ladle refining slag, but the effect of CaF_2 content (15, 20, 25, and 30 %) on the T.O. can be neglected at high C/S condition. The CaO-SiO_2-Al_2O_3-MgO system liquid inclusions can be found as the C/S < 1.3, while the formation of spinel and MgO inclusions were observed at the C/S > 1.7 for a fixed CaF_2 content (10 %). For the tundish metallurgy process, the liquid and SiO_2-rich Mn-Si-O system inclusions were found as the liquid steel reacted with rice husk ash (RHA) and RHA-CaO-SiO_2. The liquid Mn-Si-Al-O system inclusions were observed as reacted with RHA-CaO-Al_2O_3 flux. The number density of inclusions increased, decreased, and remained constant with the reaction time when the liquid steel reacted with RHA, RHA+CaO-Al_2O_3, and RHA+CaO-SiO_2 fluxes, respectively. The results indicated that the reoxidation of the liquid steel is aggravated as the RHA was used, whereas the RHA+CaO-Al_2O_3 can facilitate the removal of the inclusions during the tundish metallurgy process.

Keywords: Ladle refining, tundish metallurgy, 316L stainless steel, Si-killed steel, non-metallic inclusion, steel cleanness

1. Introduction

316L austenitic stainless steels have been widely used as engineering materials in various fields, such as aerospace, marine, and nuclear plant, because of their good formability and excellent corrosion and oxidation resistance by the surficial formation of a Cr_2O_3-based passive layer **[1-3]**. However, the formation of nonmetallic inclusions during the steelmaking process is inevitable **[4]**, which can lead to an adverse effect on the production process and deteriorate the mechanical performance of the steel products **[5-7]** when the morphology, composition, and size distribution of the nonmetallic inclusions are not precisely and properly controlled **[8]**. Therefore, the formation and change mechanism of the nonmetallic inclusions in the 316L stainless steel during the manufacturing process. According to the literature survey, numerous researchers have been made on the refining behavior of Al-killed molten steel during the ladle furnace and the continuous casting tundish processes, the fundamental studies about that of Si-killed steel are very scarce. Therefore, the effects of CaO-SiO_2-Al_2O_3-MgO-CaF_2 ladle slag and tundish fluxes, such as RHA, Flux A (RHA+CaO-SiO_2), and Flux B (RHA+CaO-Al_2O_3), on the refining behavior of Si-killed 316L stainless steel are investigated in this study.

2. Experimental

To investigate the slag-metal experiments between ladle slag and Si-killed 316L stainless steel, a high-frequency induction furnace was used in the experiments as shown in Fig. 1. 600 g of the 316L stainless steel was put in a MgO crucible. The chemical composition of 316L stainless steel after Si deoxidation is listed in Table 1. Then the crucible was then placed in a graphite susceptor (OD: 60 mm, ID: 50 mm, and H: 130 mm) which was surrounded by an insulation board to preserve heat. Before high-temperature experiments, the crucible with master alloy was positioned in a quartz tube reaction chamber (OD: 120

mm, ID: 114 mm, and H: 400 mm) of the induction furnace. The reaction chamber was vacuumed firstly using a mechanical rotary vane pump and then high purity Ar - 3% H_2 gas was continuously blown into the furnace at a fixed flow rate using a mass flow controller. Impurities in the gas were removed by purification through Drierite (W.A. Hammond Drierite Co. Ltd., Xenis, OH), silica gel, and magnesium turnings at 723 K (450 °C). The temperature of the furnace was controlled by a proportional-integral-derivative (PID) controller connected to a B-type reference thermocouple (Pt-30Rh / Pt-6Rh) and also calibrated using another B-type thermocouple before the experiments.

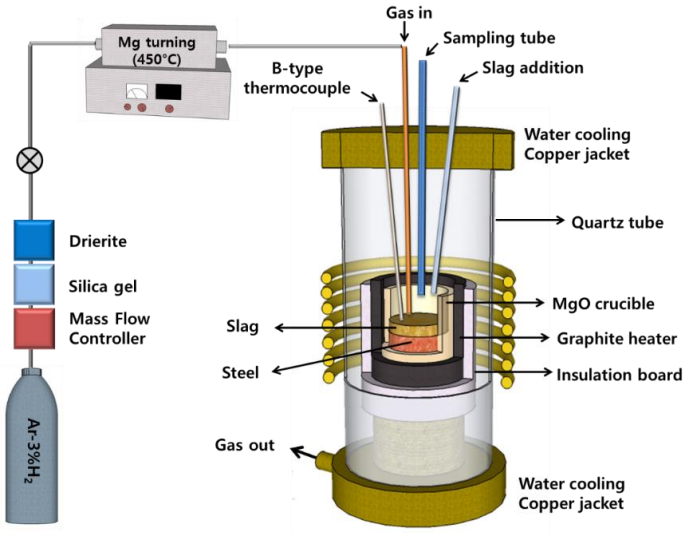

Figure 1. Schematic diagram of the experimental equipment setup.

Reagent-grade powders of CaO, SiO_2, Al_2O_3, MgO, and CaF_2 were used as raw materials. The CaO was calcined from reagent-grade $CaCO_3$ at 1273 K (1000 °C) in a muffle furnace under an air atmosphere. The thoroughly mixed powders were melted at was melted in a vertical resistance furnace at 1873 K under a high-purity Ar atmosphere to ensure complete melting and homogenization. The chemical compositions of ladle slag and tundish fluxes are listed in Table II and III, respectively. After completion of the experiments, the quenched metal samples were polished using a grinder to remove the oxide film on the surface of the metal samples and sectioned to a constant weight to reduce analytical error. The total oxygen content (T.O.) in the metal samples was analyzed by the combustion analysis method. Slag samples were ground and sized into less than 200 mesh were used for chemical analysis. The composition of metal and slag samples was determined by inductively coupled plasma-atomic emission spectroscopy (ICP-AES).

To investigate the two-dimensional morphology of non-metallic inclusion (NMI) in the alloy, pieces of the metal sample were resin-mounted and polished with 2000-grade SiC paper. Likewise, surface finishing was also conducted on the polishing machine using a 1 mm polycrystalline diamond suspension. In two-dimensional observation, the composition of NMI is not precise due to the excitation effect of the matrix phase. Three-dimensional observation after the electrolytic extraction was used to observe the exact morphology, composition, and size of inclusions in the HEAs. For this experiment, a 10 % AA solution (10 % acetylacetone, 1 % tetramethylammonium chloride, and methanol) was used as the electrolyte, and a 500 mA current was applied for 4 hours. The solution preparation method has been described elsewhere in detail **[9]**. The extracted inclusions were filtered out by a vacuum pump and laid on a membrane filter with a pore size of 0.1 μm. After the film dried, the filter was coated with platinum. Then the inclusions on the filter were evaluated by using field emission scanning electron microscopy analysis (FE-SEM; TESCAN model MIRA 3) equipped with an energy-dispersive X-ray spectroscope (EDS). The inclusion characterizations in two-dimensional, such as fraction of each type of inclusion, number density, and composition, in steel samples were determined using the automated inclusion analysis system.

Table I. The chemical compositions of Si-killed 316L stainless steel (wt.%)

C	Si	Mn	P	Ni	Cr	Mo	Cu	V	W	Ti	O	N	Al
0.01	0.42	0.74	0.030	12.13	16.40	2.04	0.28	0.06	0.04	0.003	0.009	0.003	0.0015

Table II. The chemical compositions of ladle slag used in the present study (wt.%)

Variable	Slag No.	CaO	SiO_2	Al_2O_3	MgO	CaF_2	C/S
CaO/SiO_2 ratio	1	40.0	40.0	5.0	5.0	10.0	1.0
	2	48.0	32.0	5.0	5.0	10.0	1.3
	3	50.3	29.6	5.0	5.0	10.0	1.7
	4	56.0	24.0	5.0	5.0	10.0	2.3
CaF_2 content	5	47.2	27.8	5.0	5.0	15.0	1.7
	6	44.0	25.9	5.0	5.0	20.0	1.7
	7	40.9	24.1	5.0	5.0	25.0	1.7
	8	37.8	22.2	5.0	5.0	30.0	1.7

Table III. The chemical compositions of RHA and the simulated tundish fluxes (wt.%)

Flux type	CaO	SiO_2	Al_2O_3	C	Viscosity (Pa·s) at 1773 K	Optical basicity
RHA	-	90.5	-	4.24	-	-
Flux A	51.1	43.3	-	-	0.232	0.68
Flux B	52.6	-	40.7	-	0.191	0.77

3. Results and discussion

3.1 Effect of ladle slag composition on deoxidation behaviour of Si-killed 316L stainless steel

Figure 3 represents the total oxygen content in the liquid stainless steel as a function of reaction time for various binary basicity C/S and CaF_2 contents in $CaO-SiO_2-5MgO-5Al_2O_3-CaF_2$ slag on total oxygen content in the steel at 1873 K. It is shown in Fig.2 (a) that the total oxygen content in the liquid steel decreases considerably with increasing reaction time within 30 min at the given basicity, while it stays approximately same about 25 ppm after 30 min, indicating that the deoxidation reaction reaches chemical equilibrium at 1873 K. In addition to this, the total oxygen content in the liquid steel decreases significantly as basicity changes from 1.0 to 1.7 within 30 min, whereas this effect will be nearly saturated between 1.7 and 2.3 at 1873 K. A similar behavior has been reported by the previous researchers **[10-15]**.

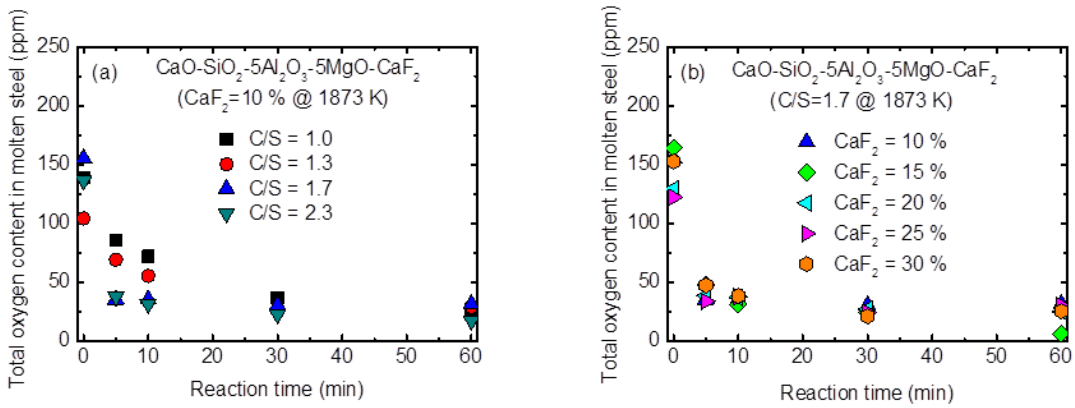

Figure 2. Effects of binary basicity C/S (a) and CaF_2 content (b) in $CaO-SiO_2-5MgO-5Al_2O_3-CaF_2$ slag on total oxygen content in the steel at 1873 K.

The effect of the slag with various CaF_2 contents on the variation of total oxygen content in the molten steel is shown in Fig.2 (b). It can be seen that the CaF_2 content has a little influence on the further reduce of total oxygen content in the liquid steel for a fixed binary basicity C/S = 1.7 at 1773 K. These results demonstrate that the changes in binary basicity in the ladle slag affect the total oxygen content in the molten steel more strongly than CaF_2 content at this temperature. Andersson et al. **[16]** presented data of plant trials to investigate the effect of CaF_2 content in $CaO-SiO_2-MgO-Al_2O_3-TiO_2-CaF_2$ ladle slag on the refining of steel and found that the presence of CaF_2 had little effect on number and type of

inclusion. The conclusion has also been approved by the work of Zheng et al., **[17]** who studied the effect of CaF_2 content on the refining ability of the high basicity CaO-$18Al_2O_3$-SiO_2-MgO-CaF_2 slag for production of Al-killed duplex stainless steel.

3.2 Effect of various tundish fluxes on reoxidation behaviour of Si-killed 316L stainless steel

The evolution of the number density of various types of inclusions in the steel samples taken at different time intervals after the addition of various fluxes is shown Fig.3. After adding the RHA, as shown in Fig.3 (a), the number density of inclusions in the steel samples increases with reaction time, and this sharp increase is caused by the serious reoxidation reaction. Nevertheless, the number density of inclusions in the steel samples stays approximately the same as reaction time passes after addition of Flux A as illustrated in Fig.3 (b), which is due to the rate of the inclusion floatation and absorption by Flux B is equal to the rate of the inclusion production by the reoxidation reaction. Compared with Figure 8(a), a contrary tendency can be found in Fig.3(c) when the molten steel reacts with Flux B. These results demonstrate that the oxidation ability of Flux B is lower than that of RHA and Flux A, and Flux B can facilitate the improvement of the cleanness of the molten steel.

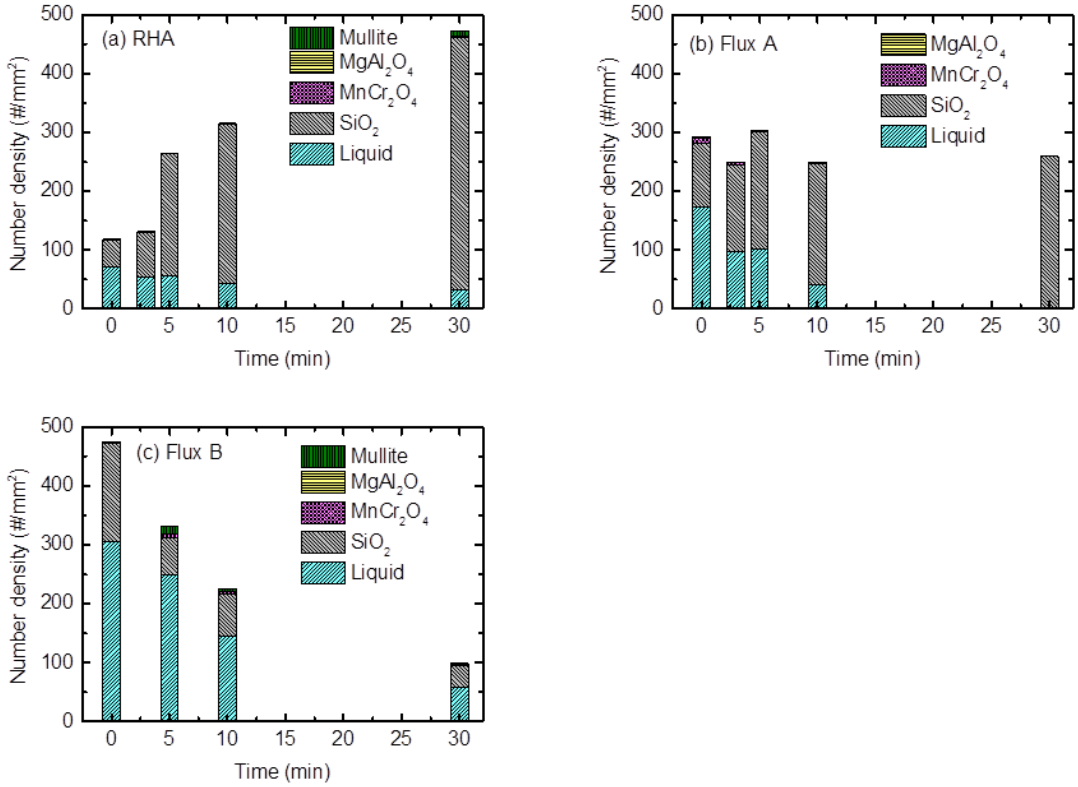

Figure 3. Number density of various types of inclusions after the addition of the various fluxes: (a) RHA, (b) Flux A, and (c) Flux B.

The ability of slag to capture solid oxide inclusion from molten steel and the total dissolution time τ of the inclusion into the slag can be expressed as follows **[18]**.

$$\tau = \frac{\rho \cdot R_0^2 \cdot 3\pi a \eta}{2kT\Delta C} \quad [1]$$

Where ρ and η represent the density and viscosity of slag, respectively. R_0, a, k, and T stand for the radius of inclusion, the ionic diameter, the Boltzmann constant (1.380649×10^{-23} J/K), and the absolute temperature (K), respectively. ΔC is the concentration difference (driving force for inclusion dissolution into slag). It can be obtained from Equation [1] that the total dissolution time of inclusion τ has a positive correlation with the ratio of slag viscosity η and concentration difference ΔC. Therefore, the liquid region of the CaO-SiO_2-Al_2O_3 ternary slag system at 1773 K calculated by

FactSage™ 7.3 software is illustrated in Fig.4. Meanwhile, the iso-$\log\left(\frac{\eta}{\Delta C}\right)$ lines are also shown in the liquid region of the CaO-SiO_2-Al_2O_3 ternary slag system to evaluate the ability of inclusion dissolution into the CaO-SiO_2-Al_2O_3 ternary slag at 1773 K. It can be seen that the $\log\left(\frac{\eta}{\Delta C}\right)$ value of Flux B is higher compared with that of Flux A along with the direction of the variation of the slag composition from 0 to 30 min, giving rise to the fact that the Flux B has a higher absorption ability of inclusion from the molten steel rather than Flux A, and the number ability of inclusions decrease with reaction time when the molten steel reacts with Flux B as shown in Fig.3 (c).

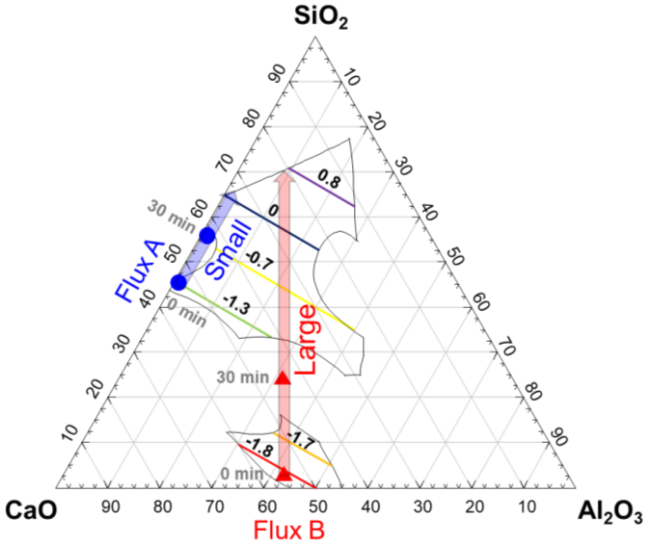

Figure 4. Iso-$\log\left(\frac{\eta}{\Delta C}\right)$ lines in liquid region of CaO-SiO_2-Al_2O_3 ternary slag system at 1773 K.

4. Conclusions

The slag-metal reactions between the Si-killed 316L stainless steel and the ladle slags with various binary basicity and CaF_2 contents as well as the fluxes RHA, RHA + CaO-SiO_2 (Flux A), and RHA + CaO-Al_2O_3 (Flux B) were conducted in an induction furnace with a MgO crucible, which is to investigate the effects of the various fluxes on the refining behavior of the liquid steel. The principal findings of the present study are summarized as follows:

1. The total oxygen content in the liquid steel decreases significantly as basicity changes from 1.0 to 1.7 within 30 min, whereas this effect will be nearly saturated between 1.7 and 2.3 at 1873 K. CaF_2 content has little influence on the further reduction of total oxygen content in the liquid steel for a fixed binary basicity C/S = 1.7 at 1873 K. These results demonstrate that the changes in binary basicity in the ladle slag affect the total oxygen content in the molten steel more strongly than CaF_2 content at this temperature.

2. The number density of non-inclusions in the steel reacted with RHA, Flux A, and Flux B increases, stays constant, and decreases as the reaction time progresses, respectively. The increase in the number density of non-metallic inclusions in the steel owing to the reoxidation of the molten steel caused by the self-dissolution reaction of SiO_2 in RHA. However, the Flux B has a higher value of $\log\left(\frac{\eta}{\Delta C}\right)$ and lower SiO_2 activity compared with Flux A, *viz.*, the inclusion absorbs ability is stronger than the oxidation ability of the Flux B, which is responsible for the drop in the number density of non-metallic inclusions in the liquid steel.

REFERENCES

[1] X.H. Chen, J. Lu, L. Lu, K. Lu, Tensile properties of a nanocrystalline 316L austenitic stainless steel, Scr. Mater., 52 (2005) pp. 1039-1044.

[2] H. Ueno, K. Kakihata, Y. Kaneko, S. Hashimoto, A. Vinogradov, Enhanced fatigue properties of nanostructured austenitic SUS 316L stainless steel, Acta Mater., 59 (2011) pp. 7060-7069.

[3] C. Wang, P. Zhu, F. Wang, Y.H. Lu, T. Shoji, Anisotropy of microstructure and corrosion resistance of 316L stainless steel fabricated by wire and arc additive manufacturing, Corros. Sci., 206 (2022) pp. 110549.

[4] B.H. Reis, W.V. Bielefeldt, A.C.F. Vilela, Absorption of non-metallic inclusions by steelmaking slags - A Review, J. Mater. Res. Technol., 3 (2014) pp. 179-185.

[5] J.H. Park, H. Todoroki, Control of $MgO\text{-}Al_2O_3$ spinel inclusions in stainless steels, ISIJ Int., 50 (2010) pp. 1333-1346.

[6] J.H. Park, Y. Kang, Inclusions in stainless steels − A review, Steel Res. Int., 88 (2017) pp. 1700130.

[7] J.H. Park, L. Zhang, Kinetic modeling of nonmetallic inclusions behavior in molten steel: A review, Metall. Mater. Trans. B, 51 (2020) pp. 2453-2482.

[8] L. Zhang, B.G. Thomas, State of the art in evaluation and control of steel cleanliness, ISIJ Int., 43 (2003) pp. 271-291.

[9] J.H. Park, D.-J. Kim, D.J. Min, Characterization of nonmetallic inclusions in high-manganese and aluminum-alloyed austenitic steels, Metall. Mater. Trans. A, 43 (2012) pp. 2316-2324.

[10] M. Jiang, X. Wang, B. Chen, W. Wang, Laboratory study on evolution mechanisms of non-metallic inclusions in high strength alloyed steel refined by high basicity slag, ISIJ Int., 50 (2010) pp. 95-104.

[11] W.J. Ma, Y.P. Bao, M. Wang, D.W. Zhao, Influence of slag composition on bearing steel cleanness, Ironmaking Steelmaking, 41 (2013) pp. 26-30.

[12] Y. Hu, W.Q. Chen, Influence of refining slag composition on cleanness and fatigue life of 60Si2MnA spring steel, Ironmaking Steelmaking, 43 (2016) pp. 340-350.

[13] Y. Ren, L. Zhang, W. Fang, S. Shao, J. Yang, W. Mao, Effect of slag composition on inclusions in Si-deoxidized 18Cr-8Ni stainless steels, Metall. Mater. Trans. B, 47 (2016) pp. 1024-1034.

[14] Y. Li, C. Chen, Z. Jiang, M. Sun, H. Hu, H. Li, Application of alkali oxides in LF refining slag for enhancing inclusion removal in C96V saw wire steel, ISIJ Int., 58 (2018) pp. 1232-1241.

[15] S.C. Duan, X. Shi, M.C. Zhang, B. Li, W.S. Yang, F. Wang, H.J. Guo, J. Guo, Effect of slag composition on the deoxidation and desulfurization of Inconel 718 superalloy by ESR type slag without deoxidizer addition, Metall. Mater. Trans. B, 51 (2020) pp. 353-364.

[16] E. Andersson, D. Sichen, The effect of CaF_2 in the slag in ladle refining, Steel Res. Int., 80 (2009) pp. 544-551.

[17] L. Zheng, H. Li, X. Wang, Z. Jiang, H. Feng, Effect of CaF_2 on viscosity and refining ability of highly basic slags for duplex stainless steel, ISIJ Int., 61 (2021) pp. 1784-1793.

[18] M. Valdez, G.S. Shannon, S. Sridhar, The ability of slags to absorb solid oxide inclusions, ISIJ Int., 46 (2006) pp. 450-457.